Int. J. Electrochem. Sci., 12 **(2017)** 4898 – 4914, doi: 10.20964/2017.06.74

International Journal of ELECTROCHEMICAL SCIENCE
www.electrochemsci.org

Electrodeposition of Nanostructured ZnO Photoanodes for Their Application in the Oxygen Evolution Reaction

F. D. Ruiz-Ocampo[1], *J. M. Zapien-Rodríguez*[1], *O. Burgara-Montero*[1], *E. A. Escoto-Sotelo*[1], *F. A. Núñez-Pérez*[1,*], *and J. C. Ballesteros-Pacheco*[1,*]

[1] Universidad Politécnica de Lázaro Cárdenas, Laboratorio de Sustentabilidad Energética, Av. Galeanas S/N, Colonia Las 600 Casas S/N, C.P. 60950, Lázaro Cárdenas, Michoacán, México.
[*]E-mail: jballesteros_pacheco@yahoo.com.mx, phd_paco@hotmail.com

Received: 22 February 2017 / *Accepted:* 12 April 2017 / *Published:* 12 May 2017

In this work it is reported by first time the galvanostatic electrodeposition of nanostructured ZnO films on indium tin oxide (ITO) substrates from oxygenated-neutral solution containing $Zn(CH_3COO)_2$ and $K(CH_3COO)$ at different temperature from 50 to 70°C. Morphological, structural, UV-vis spectra, photoluminescence spectra and photoelectrochemical tests of the electrodeposited ZnO films were measured. The synthesis conditions studied were the parameters temperature and applied current density. SEM results show ZnO films with grains of hexagonal shape, which present different grain size (150-600 nm) as a function of the studied parameters. The optical properties of ZnO films show absorption in the UV-visible region with band gap energy values from 2.92 to 3.15 eV. Through a XRD analysis, we show that the electrodeposition conditions also have an effect in the intensity of (002) polar and (100) no polar planes of electrodeposited ZnO films. Additional results by photoluminescence indicate presence of oxygen vacancies in the electrodeposited ZnO films, which is a factor considered as responsible of enhance electroactivity of ZnO films for oxygen evolution reaction in visible region. Calculations of overall solar to hydrogen efficiency for electrodeposited ZnO films indicate a maximum value of approximately $\eta = 0.65\%$ for ZnO film obtained at $j = -1.0$ mA cm^{-2} and 70°C.

Keywords: Oxygen Evolution Reaction; Zinc Oxide; Electrodeposition; Electrocatalyst.

1. INTRODUCTION

The electrochemical systems based in the use of sun, water and new materials are a good option for production of alternative energy. Among several options of electrochemical systems for storage and/or conversion of energy are lithium-ion batteries, metal extraction, electrolyzers and solar-driven water-splitting devices, which involve different chemical reactions. The oxygen evolution reaction

(OER) is a common electrochemical reaction involved in the named electrochemical devices. The OER is a complicated process that require the transfer of four electrons and generation of four protons as follow [1]:

$$2H_2O \rightarrow O_2 + 4H^+ + 4e^- \quad (1)$$

A disadvantage of the OER is its large overpotential due to the slow kinetic, which has provoked to research on design new electrocatalysts with high electrocatalytic activity and with the lowest overpotential for carry out this process. To the present time, RuO_2, IrO_2 and PtO_2 are reported as the best anodes for be used in the OER, which contain noble elements that are expensive and few abundant [1, 2].

However, some spinel oxides, perovskite oxides, layered hydroxides and layered double hydroxides such as Co_3O_4, $NiCo_2O_4$, $LaCoO_3$, NiOOH, NiFe-LDH, NiCO-LDH, ZnCo-LDH [3-14] are reported as good electrocatalysts for the OER. These oxides are principally composed of oxygen atoms bound to transition metals, which are cheap and abundant metals. Its main disadvantage is due to their low chemical stability, which is a limitation to the application of these at an industrial level. Among the various alternatives of electrocatalysts, zinc oxide (ZnO) is a compound considered as an excellent candidate for its application in the OER. The principal characteristics of ZnO are its high chemical stability, high electrocatalytic activity and ability to absorption of solar irradiation [15-22].

Recent studies on ZnO indicate that this semiconductor material is a promising candidate for its application as electrocatalyst in hydrogen production by photoelectrochemical water splitting [15-22]. ZnO characteristics that make it a good candidate as electrocatalyst are its wide variety of surface planes polar and non-polar, which affect the surface energy of this material and influence their electrocatalytic properties. Structural defects in ZnO such as oxygen vacancies also influence their electrocatalytic properties. Additionally, the investigations report for ZnO a direct band gap energy from 2.9 to 3.4 eV, a large exciton binding energy (60 meV), good electrical conductivity, low cost and non-toxicity [23].

ZnO is used as a photocatalyst and/or photoanode under UV light due to its wide band gap. However, the possible application of ZnO as a photocatalyst/absorber in the visible light region has been reported by several research groups in the last years [24-28]. The strategies employed by these researches to transform ZnO in a vis-absorber are doping with different metals, non-metals or the mixture with other oxides, as well as the generation of oxygen vacancies [24-28]. Particularly, vacancies are a kind of structural defects that can act as electron trap centers decreasing recombination rate of electron-hole pair. In the case of oxygen vacancies has been reported that these help in the band gap narrowing by producing an impurity level near the valence band [24–29].

In the literature [23, 28] are reported a variety of methods for preparation of ZnO in powder or thin films. In the case of ZnO films, these are usually deposited by techniques such as magnetron sputtering, spray pyrolysis, molecular beam epitaxy and electrochemical deposition. Through these methods zinc oxide thin films can be obtained with a diversity of ZnO nanostructures i.e. wires, rods, tubes, sheets, pencils, etc. Nanostructures offer advantages over bulk materials due to their short lateral diffusion length and low reflectivity [23, 26-28].

The electrodeposition is a low cost alternative that offers a high degree of control during the nucleation and growth and it does not require dangerous experimental conditions. For

electrodeposition of ZnO is required the presence of OH^- radicals, which are principally obtained from dissolved molecular oxygen or nitrate precursor [23, 28]. The $ZnCl_2$-KCl and $Zn(NO_3)_2$-KNO_3 aqueous systems have been typically employed as zinc and electrolytic conductivity sources in the majority of the works previously reported [9]. However, few investigations have been carried out using alternative zinc sources, for example, the use of acetates, which have showed that is possible to obtain ZnO films by electrodeposition with good optical properties [30–33].

Therefore, in this work we here present for the first time the electrochemical preparation of ZnO thin films through galvanostatic electrodeposition from oxygenated solution containing 5 mM $Zn(CH_3COO)_2$ and 0.1 M $K(CH_3COO)$ at pH 7.0. The studied parameters during the electrodeposition process were bath temperature and applied current. The application of the ZnO films was as electrocatalyst for oxygen evolution reaction.

2. EXPERIMENTAL

2.1. ZnO films electrodeposition

ZnO films were deposited on ITO substrates (Sigma-Aldrich, 15-25 Ω/sq), via galvanostatic electrodeposition from electrolytic solution containing 5 mM $Zn(CH_3COO)_2$ and 0.1 M $K(CH_3COO)$ and KOH was used to adjust the pH to 7. All solutions were prepared with deionized water (18 MΩ cm) and using analytical grade reagents purchased from Sigma-Aldrich. All electrochemical experiments were carried out in a conventional three-electrode cell system. The electrochemical methods used in this work were cyclic voltammetry, chronoamperometry and chronopotentiometry. Platinum wire and Ag/AgCl electrode were used as counter and reference electrodes, respectively. ITO substrates were used as working electrode, which previously were cleaned and sonicated in acetone, ethanol and deionized water for 10 minutes in each medium, respectively. Before the electrochemical experiments, the electrolytic solution was saturated by direct gas bubbling with extra dry 99.5% pure O_2 during 1 hour. The applied current densities were -1.0, -1.5 and -2.0 mA cm^{-2} during 1800 seconds at different bath temperature: 50, 60 and 70 °C. The electrochemical tests were conducted with potentiostat/galvanostat AUTOLAB PGSTAT302N coupled to a computer with the NOVA software for data acquisition. In this work all potentials are referred with respect to the Ag/AgCl electrode.

2.2 Structural, morphological and optical characterization of the electrodeposited films

Crystal structure of electrodeposited films was examined by X-ray diffraction using Cu Kα radiation (= 1.5406 Å) operating with grazing angle in a Siemens D5000 X-ray diffractometer, XRD data were acquired from 2θ = 30° to 70° (step 0.02°, scan rate 2° min^{-1}). The surface morphology of the electrodeposited films obtained was observed using a FEI Nova 200 NanoSEM field emission scanning electron microscope. Diffuse reflectance UV–Vis–NIR spectra were run at room temperature on a Cary 5000 UV-Vis spectrophotometer. UV–Vis spectra are reported in the Tauc's plot to determinate the optical band gap (Eg) using the transformed diffuse reflectance technique according to

the Kubelka-Munk theory [34, 35]. The room temperature photoluminescence (PL) spectra of ZnO were carried out in a Spectrofluorophotometer (RF-6000, SHIMADZU) with an excitation wavelength of 340 nm in order to further elucidate the kind of emission spectrum obtained for electrodeposited ZnO films.

2.3. Photoelectrochemical characterization.

Photoelectrochemical experiments were performed in a quartz electrochemical cell using the as-prepared ZnO films (1.0 cm^2), Pt wire and Ag/AgCl as working, counter and reference electrodes, respectively. The chemical composition of the solution was 0.5 M Na_2SO_4 without sacrificial reagents or co-catalyst. Before each photoelectrochemical experiment N_2 gas was bubbled during 20 minutes in the solution in order to remove atmospheric oxygen. The chemical stability of prepared ZnO films as photoanodes was evaluated by chronoamperometric (CA) measurements under simulated sunlight on-off cycles illumination. The lamp's shutter was opened and closed each 300 seconds during a total time of 3600 seconds. The photoelectrochemical performance of ZnO films during the water splitting reaction was analyzed by linear sweep voltammetry (LSV). The LSV was performed at a scan rate of 10 mV s^{-1} from open circuit potential (E_{oc}) to 0.5 V under simulated sunlight illumination (Sol1A Newport solar simulator, 450 W Xe lamp). Solar to hydrogen efficiency was calculated for all samples from current–potential curves (I *vs* E).

3. RESULTS

3.1 Thermodynamic study of zinc-acetate-water system

With the finality to understand the deposition solution chemistry and the zinc species involved in the electrodeposition process, a study on the thermodynamic stability of all the chemical species contained in the solution was carried out by constructing a species repartition diagram.

The acetic acid has a pKa value of 4.77 and it can be dissociated to H^+ and CH_3COO^- ions [36]. Depending on zinc concentration, acetate concentration and pH, the acetate ions can successively replace water molecules in zinc's coordination octahedron, forming three possible zinc–acetate complexes: $Zn(Ac)^+$, $Zn(Ac)_2$ and $Zn(Ac)_3^-$, where $Ac^- = CH_3COO^-$. In aqueous solution, Zn(II) soluble species may be: free Zn^{2+} ions, zinc-hydroxide and zinc-acetate complexes. The equilibrium concentrations of each of these complexes are represented by the next Equation:

$$Zn^{2+} + iL^- \leftrightarrow ZnL_i^{(2-i)} \quad (1)$$

The Equation 1 is characterized by its stability constant $\beta_i^{L^-}$:

$$\beta_i^{L^-} = \frac{\left[ZnL_i^{(2-i)}\right]}{[L^-]^i[Zn^{2+}]} \quad (2)$$

Where L^- represents the type ligand (OH^- or Ac^-) and *i* is the coordination number. All stability constants (reported in Table 1) were obtained from literature [37, 38].

Table 1. Equilibrium constants for the overall formation of complexes in the zinc-acetate-water system obtained from the literature [28, 29].

Ligand	Ac^-			OH^-			
	1	2	3	1	2	3	4
Formation constant (β_i^L)	0.079	0.123	0.012	4.4	11.3	13.7	16.6

Using stability constants it is possible to calculate the ratio between soluble zinc species and total zinc concentration in solution. The species repartition-pH diagram was computed using the definition of complexation coefficient of Zn (II), $\alpha_{zn(L=\ Ac^-,\ OH^-)}$. It is defined as: the ratio C_{Zn} / $[Zn^{2+}]$, where C_{Zn} is the total concentration of zinc including all complexes and $[Zn^{2+}]$ is the concentration of free zinc cations [39].

The Figure 1 shows the species repartition diagram obtained for the $Zn^{2+}/Ac^-/H_2O$ system. This diagram shows the mole fraction of Zn species present as a function of pH. $Zn^{2+}, Zn(Ac)^+$ and $Zn(Ac)_2$ species appear in the pH range between 0 and 7, where the Zn^{2+} ions become the predominant species. No zinc acetate complexes are observed at pH value above 7.2. For a pH range of 8.3-11.2, $Zn(OH)_2$ is the predominant complex. At pH values above 11.2, $Zn(OH)_4^{2-}$ are the predominant species.

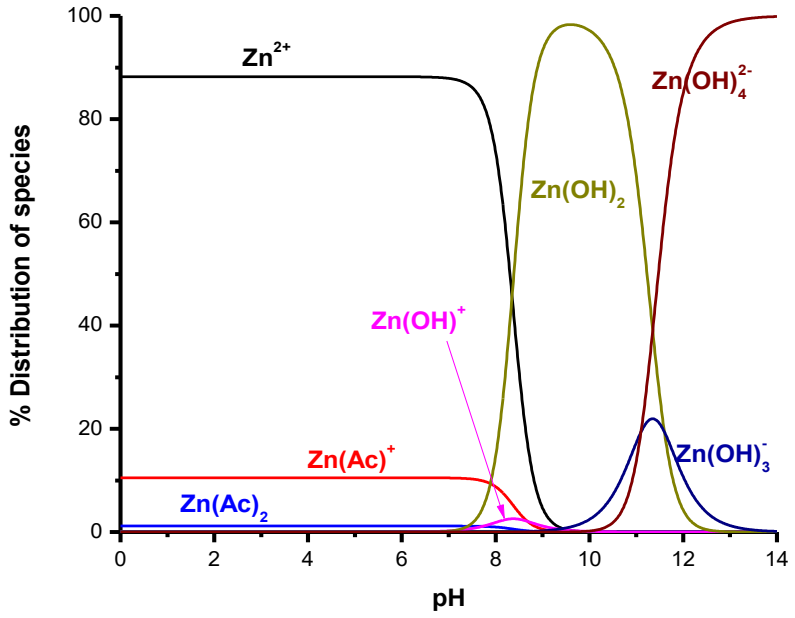

Figure 1. Species distribution diagrams as a function of pH for the $Zn^{2+}/Cl^-/CH_3COO^-/H_2O$ system.

In the literature [23, 28, 40, 41] is widely reported that the formation of ZnO is carried out from aqueous solution containing $ZnCl_2$, KCl and oxygen as electrolyte through the next reaction:

$$Zn^{2+} + \frac{1}{2}O_2 + 2e^- \rightarrow ZnO \qquad (3)$$

Therefore, from results obtained it is possible to propose that the Zn^{2+}, $Zn(OH)_2$ and $Zn(OH)_4^{2-}$ complexes are the predominant species in the $Zn^{2+}/Ac^-/H_2O$ system. However, the free Ac^- ions in the solution are available to act as an additive during the formation of ZnO.

3.2. Electrochemical preparation of ZnO films

Figure 2 shows a comparison between voltammograms on ITO substrate with and without dissolved oxygen in the solution represented by dashed and solid lines, respectively. For both cases, the scan rate begin in negative direction from open circuit potential at 10 mV s^{-1}. The dashed vertical line corresponds to the theoretical value of equilibrium potential calculated for electrochemical reduction of Zn^{2+} to Zn at pH 7.0 using Nernst equation. During the potential scan in negative direction, the voltammogram represented by solid curve (without dissolved oxygen) in Figure 2 shows a negligible current in the potential range from -0.1 to -0.84 V, which is indicating that none reaction is occurring.

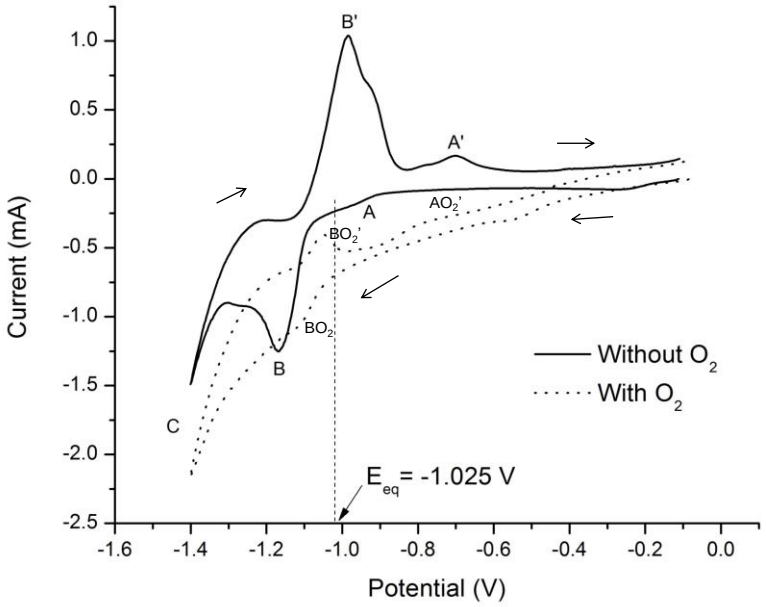

Figure 2. a) Cyclic Voltammograms on ITO substrate recorded from aqueous zinc acetate solution, with and without O_2.

For potential values more negative than -0.84 V it is possible to observe a slight rise in cathodic current, labeled as peak A. Based on our thermodynamic calculations the peak A is occurring at potential values more positive than the equilibrium potential calculated from Nernst equation (E_{eq} = -1.025 V). In literature, this behavior has been associated to a phenomenon known as under potential deposition (UPD) of Zn [39, 42, 43]. We proposal that UPD process of Zn on ITO is occurring because the work function of zinc and ITO are approximately 3.6 and 4.7 eV [39, 44], respectively. Kolb et al. [45] have proposed that when the work function of a metal being electrodeposited is lower than that of

the substrate metal, the electrodeposition may occur at a potential more positive than the equilibrium potential, a phenomenon called underpotential deposition (UPD). For lower potential values than -1.08 V, it is clear to observe a great increment in the cathodic current to produce the peak B indicating that the deposition of metallic zinc on the ITO substrate has occurred. The experimental value for equilibrium potential of electrodeposition of zinc was taken as -1.08 V. The difference between experimental and theoretical value of equilibrium potential is approximately 55 mV. From Figure 2 it is clear to observe that the values of potential peak (E_{pB}) and current peak (i_{pB}) are -1.16 V and -1.25 mA, respectively. Finally, in the Figure 2 is possible to observe a new increment in the cathodic current for potential values more negative than -1.30 V, which was associated to hydrogen evolution reaction (HER).

When scan rate was inverted in positive direction at -1.4 V, the peak B' and peak A' appear with values of peak potential of -0.98 V and -0.7 V, respectively. The presence of these two peaks indicates the dissolution of two different species of zinc formed during the negative potential scan. Figure 2 shows that the current peak ($i_{pB'}$) associated to peak B' is 1.1 mA.

Voltammogram represented by the dashed curve in Figure 2 shows the effect of the oxygen-saturated solution on voltammetric response. The incorporation of oxygen in the solution provokes that both current branches of voltammogram present negative current values in all potential range studied. Nevertheless, it is possible to detect the formation of signals associated to oxidation and reduction of the zinc species.

Table 2. Different conditions of electrodeposition of ZnO from a solution containing zinc acetate and potassium acetate at pH = 7.

T / °C	j / mA cm^{-2}	ZnO film
50		ZnO1
60	-1.0	ZnO2
70		ZnO3
50		ZnO4
60	-1.5	ZnO5
70		ZnO6
50		ZnO7
60	-2.0	ZnO8
70		ZnO9

During the potential scan in negative direction, voltammetric curve presents the peak B_{O2}, which has a value of potential peak (E_{pBO2}) of about -1.09 V. It is important to note that the peak B_{O2}

shift towards potential values more positive than the peak B; in the literature [2] this behavior is characteristic of a electrochemical reaction followed by a chemical reaction. This electrochemical-chemical scheme is due to the electrochemical reduction of molecular oxygen followed by the chemical reaction of formation of ZnO.

The current obtained during positive potential scan displays the anodic peaks BO_2' and AO_2' at potential values of approximately -1.05 and -0.80 V, respectively. These peaks correspond with the dissolution of the two species of zinc formed during the scan in negative direction. Similar results have been mentioned by Nişancı et al. [42] in where they reported the presence of zinc UPD during the formation of ZnO. From the results shown in Figure 2 in presence of molecular oxygen, were selected three current values to formation of ZnO on ITO substrate. These values were j = - 1.0, -1.5 and -2.0 mA cm^{-2}. Additionally, a study of effect of temperature (in the range 50-70 °C) during the electrochemical synthesis of ZnO also was analyzed. Table 2 shows the conditions and labels for each one of the films of ZnO synthesized by electrochemical method.

3.3. Structural Characterization

Figure 3 shows the XRD patterns corresponding to the electrodeposited films at different current density and temperature, see Table 2. In the nine samples, the diffraction peaks were consistent with crystalline ZnO in the wurzite structure (PDF 01-089-1397). In Figure 3, it is possible to detect the presence of signals due to ITO substrate (PDF 03-065-3358). Additionally, all patterns DRX indicate the presence of (002) and (101) peaks corresponding to hexagonal Zn. The presence of this second phase is associated to the electrodeposition of Zn UPD. A quantitative analysis of both crystalline phase of zinc (ZnO and Zn) was carried out by numerical integration of area under each peak; the results indicate a percentage of relative phase for Zn metallic of around 5%.

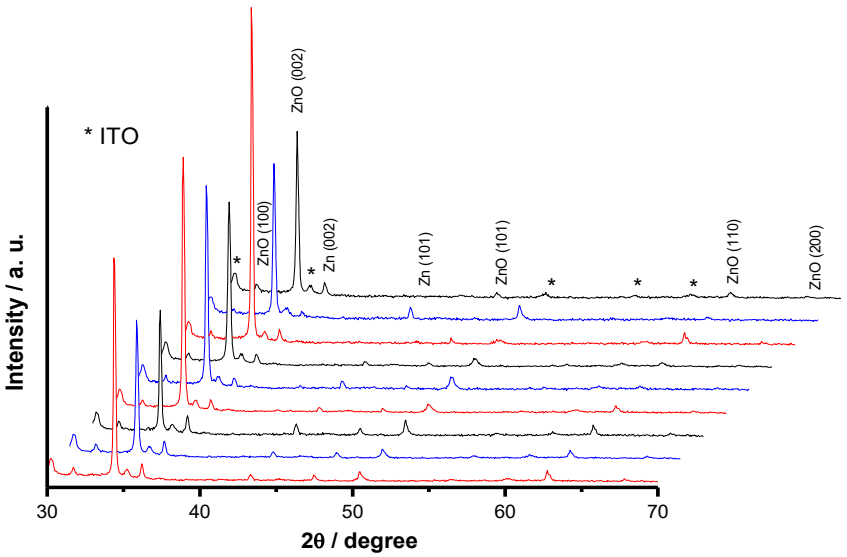

Figure 3. XRD patterns of electrodeposited ZnOfilms at different temperature and applied current: a) ZnO1, b) ZnO2, c) ZnO3, d) ZnO4, e) ZnO5, f) ZnO6, g) ZnO7, h) ZnO8 and i) ZnO9.

Figure 4 shows the diffraction intensity ratios of (002) polar plane to (100) non-polar plane ($I_{(002)}/I_{(100)}$) measured from XRD patterns. It is clear to observe that the $I_{(002)}/I_{(100)}$ value increases as the value of cathodic density current was increased during the electrodeposition process. Opposite behavior was observed for the temperature, in where the $I_{(002)}/I_{(100)}$ value increases as the temperature was increased. From these results the highest value of $I_{(002)}/I_{(100)}$ proportion correspond to the ZnO3 film. In the literature has been reported that when larger fraction of (002) polar planes is achieved, it means that a higher concentration of oxygen vacancies in ZnO have been generated [46].

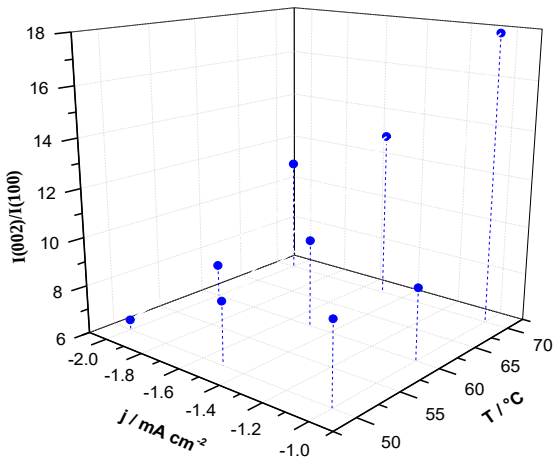

Figure 4. I(002)/I(100) ratios obtained from Figure 3 for all ZnO films.

3.4. Morphological Characterization

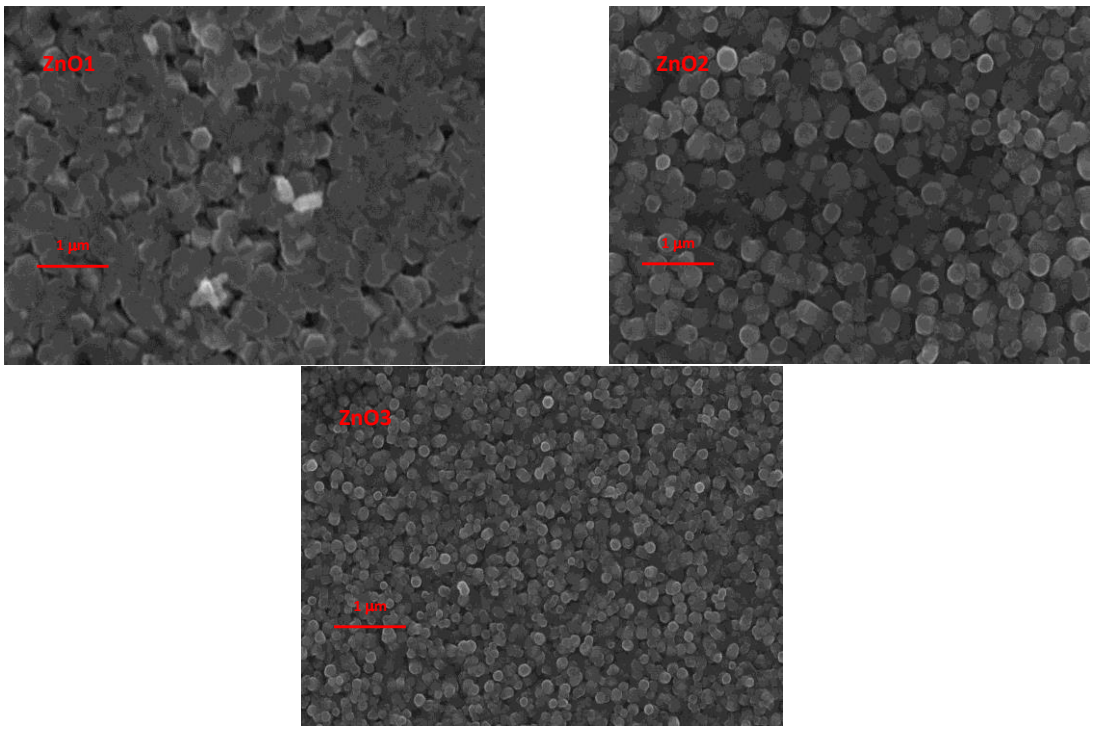

A

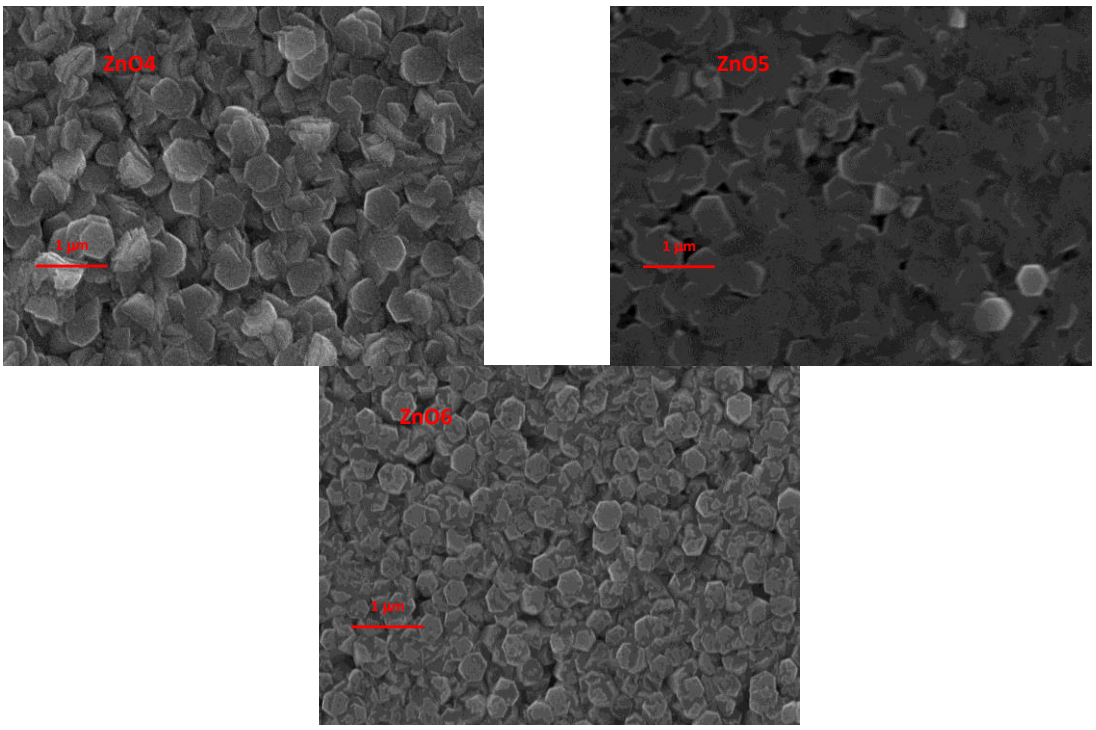

B

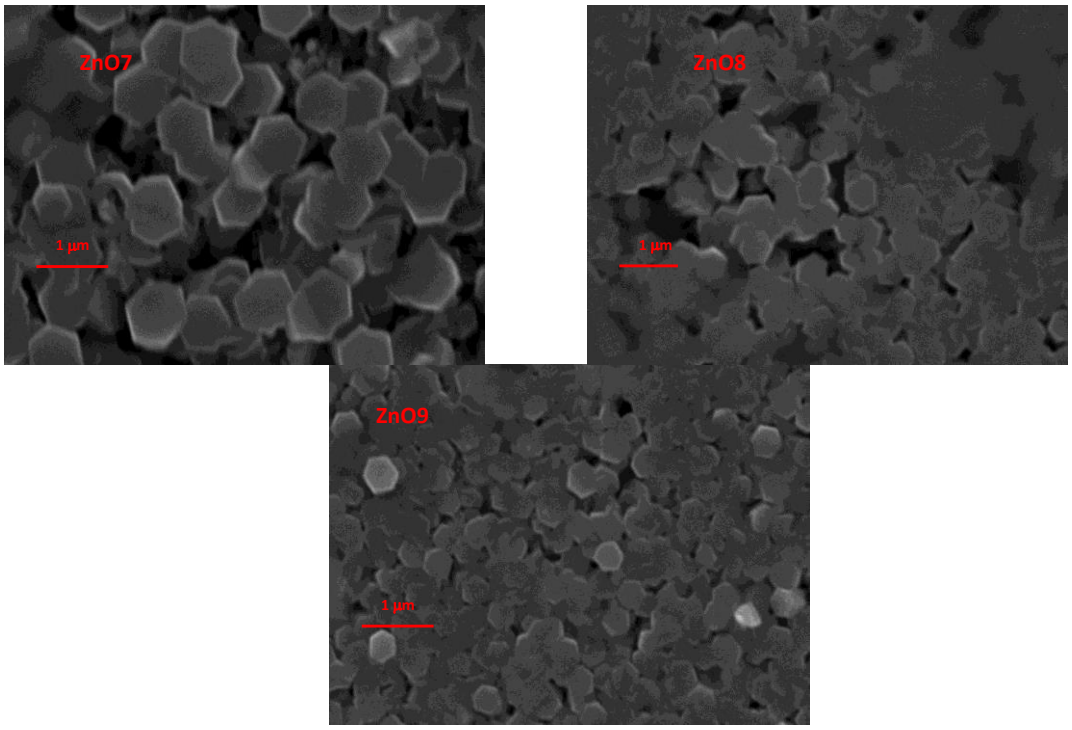

C

Figure 5. SEM images of electrodeposited ZnO films at different temperature and applied current: a) ZnO1, b) ZnO2, c) ZnO3, d) ZnO4, e) ZnO5, f) ZnO6, g) ZnO7, h) ZnO8 and i) ZnO9.

Figure 5 shows the morphologies of the all films electrodeposited and it clear to observe that a well-defined hexagonal morphology was grown. However, the grain size is depending on the electrodeposition conditions. The grains sizes for the ZnO films were found to range from 150 to 600 nm. A comparative analysis of the different grains sizes for the ZnO films indicates a synergic effect of

the parameters temperature and current density. For the case of the bath temperature, the results SEM show that when this parameter increase from 50 to 70°C, under conditions of constant current density, the grain size in ZnO films is diminished. However, in the case of the electrodeposition under isothermal conditions, the images SEM show that the grain size in ZnO films increases as the current density value is increased. These results demonstrate that the film ZnO3 contain structures with the smallest grain size of approximately 150 nm. From results XRD and SEM, it is important to note that the formation of ZnO structures with smaller grain size provokes an increase in the $I_{(002)}/I_{(100)}$ value, which in turn provoke an increase in the generation of oxygen vacancies.

3.5. Optical Characterization

Figure 6 shows the Tauc's plots for all ZnO films. The band gap energy was also determined from extrapolation of a straight line fitted to the linear part of all curves in Figure 6, in the range between 354 and 388 nm. The results indicate a variation in the values of Eg between 2.92 and 3.15 eV for each ZnO film. The comparison of these results show that smallest band gap energy corresponds to the sample ZnO3. It is important to comment that the Eg value is depending on the selected wavelength range. A comparative analysis of these results and the observed in Figure 4 are indicating that a high value of $I_{(002)}/I_{(100)}$ provoke a decrease in the value of band gap, which is provoked by generation of oxygen vacancies in the ZnO films. Wang et al. [24], reported a close relationship between band gap narrowing and oxygen vacancies concentration. They have reported that when lots of oxygen vacancies are present, the impurity states become more delocalized, overlapping with the valence band edge and raising its position, producing red-shifted absorption [24].

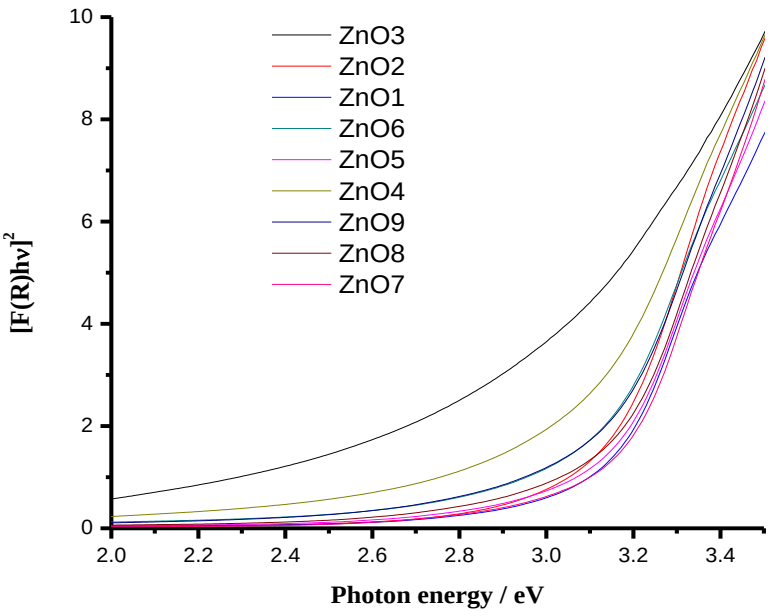

Figure 6. Tauc´s Plot of electrodeposited ZnO films at different temperature and applied current: a) ZnO1, b) ZnO2, c) ZnO3, d) ZnO4, e) ZnO5, f) ZnO6, g) ZnO7, h) ZnO8 and i) ZnO9.

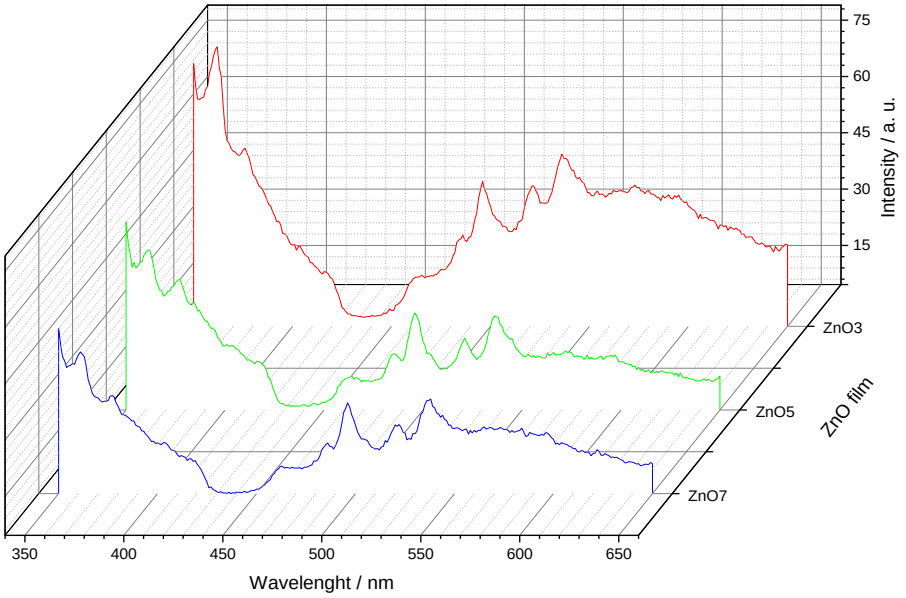

Figure 7. Room temperature PL spectra of electrodeposited ZnO films at different temperature and applied current: a) ZnO1, b) ZnO2, c) ZnO3, d) ZnO4, e) ZnO5, f) ZnO6, g) ZnO7, h) ZnO8 and i) ZnO9.

The presence of these intrinsic defects in ZnO was confirmed by photoluminescence (PL) experiments. Figure 7 shows the typical PL spectra obtained for ZnO samples on ITO substrate. All deposited films exhibited similar intensities of UV (exciton) emissions (360 nm) and different intensities for visible (deep level) emissions with peaks at 484, 495, 521, 544 and 596 nm. These deep level emissions are generally attributed to defects in the crystal structure like zinc or oxygen vacancies and interstitial or antisite oxygen [24–26, 46, 47].

The green luminescence bands around 510 nm are generally attributed to recombination of electrons in singly ionized oxygen vacancy with holes in the valence band or electron transition from conduction band to zinc vacancies level which is situated 0.9 eV above the valence band [23]. The most intense visible signal was exhibited by the sample with highest $I_{(002)}/I_{(100)}$ ratio, which also showed red-shift in absorption edge indicating greater portion of oxygen vacancies. In general, samples electrodeposited at 70 ^{o}C shown higher relative intensity than films obtained at 50 and 60 ^{o}C. This behavior can be attributed to the kinetic energy of atoms in ZnO lattice, which is relative low and the absorption of oxygen is higher than its desorption, when the electrodeposition of ZnO is occurring [48]. Therefore, the decreased intensity of visible emissions can be explained due to oxygen entering into crystal lattice sites improving stoichiometry and crystalline quality, as it was reported by Zhou et al. [49]. The bare ITO substrate does not show any visible PL response.

On the other hand, it has been reported that oxygen vacancies enhance charge transportation by reducing electron-hole recombination rates, which provoke an increase in the parameter known as overall solar to hydrogen efficiency (STH) [34, 35]. However, when the concentration of oxygen vacancies is too high, bulk vacancies in the ZnO lattice are easily generated and act as a recombination

center of electron-hole pairs resulting in the decrease of the photocatalytic activity [24, 25]. Therefore, ZnO materials with optimum oxygen vacancies amount may show higher photoelectrochemical perfomance.

3.6. Photoelectrochemical evaluation

Transient photocurrents were recorded at open circuit potential under simulated sunlight on/off cycles. The chemical stability of ZnO is a key factor for its application in high efficiency PEC devices [22, 23]. As can be seen in Figure 8 the photoresponse of ZnO films was fast and remained constant during 3000 s, when ZnO was used as photoelectrode. This Figure also shows that under illumination, the photocurrent for all samples increases, and when light is turned off, this photoresponse returns to initial current. After light was turned on, immediately a maximum photocurrent is achieved, which decay within 50 s until reaches a steady photocurrent value. This behavior is due to the formation of a diffusion layer at the photoelectrode-solution interface. From all curves in Figure 8, the highest photocurrent values were 110, 150 and 210 µA cm^{-2} for ZnO films obtained at 70° and -2.0, -1.5 and -1.0 mA cm^{-2}, respectively. These results indicate that ZnO with grain size of 150 nm leaded to highest photocurrent values, associated to oxygen evolution reaction under solar simulated irradiation.

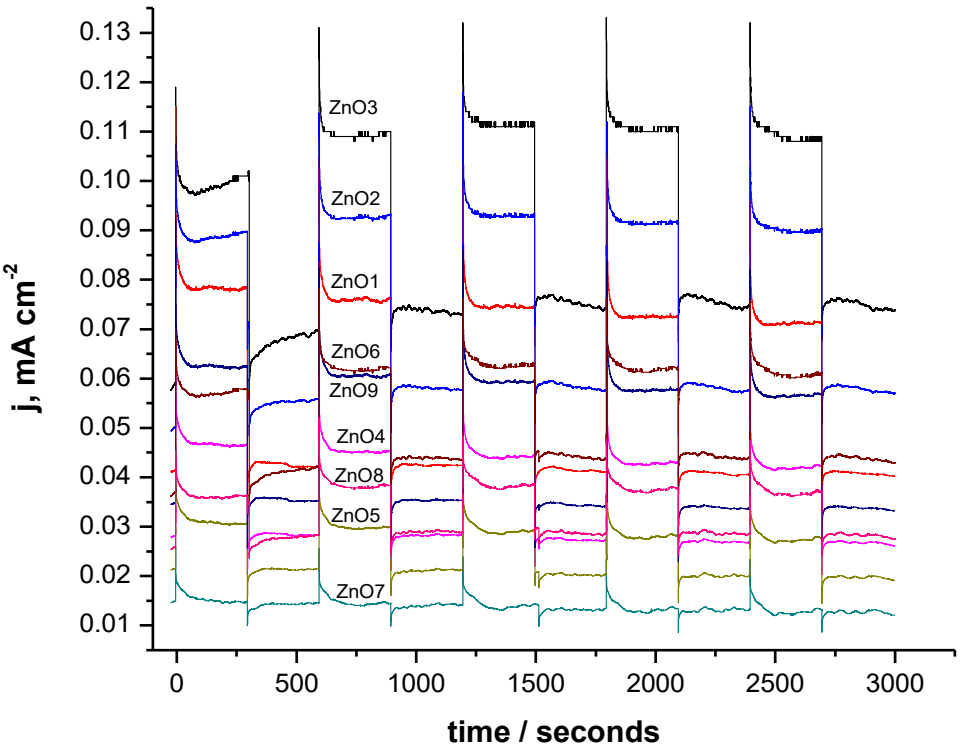

Figure 8. Photocurrent–time curves of electrodeposited ZnO films at different temperature and applied current: a) ZnO1, b) ZnO2, c) ZnO3, d) ZnO4, e) ZnO5, f) ZnO6, g) ZnO7, h) ZnO8 and i) ZnO9.

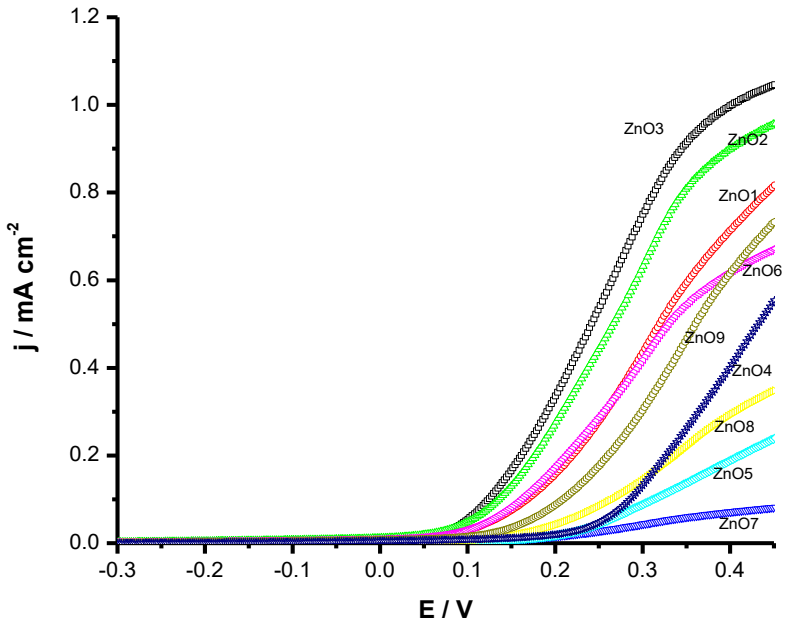

Figure 9. Linear sweep voltammograms of electrodeposited ZnO films at different temperature and applied current: a) ZnO1, b) ZnO2, c) ZnO3, d) ZnO4, e) ZnO5, f) ZnO6, g) ZnO7, h) ZnO8 and i) ZnO9.

Electrochemical measurements, by LSV technique, were carried out with the finality to evaluate the photoelectrochemical behavior of ZnO films under simulated sunlight irradiation. The photocurrent versus potential curves obtained for all ZnO films are shown in Figure 9. All linear sweep voltammograms show that the photocurrent values rapidly increase for potential values higher than 0.1 V. From comparison of all voltammograms, it is possible to note that the film ZnO3 presented the highest photocurrent.

Thus, when this ZnO film was influenced by the electrical field generated by external applied bias potential an increment in the amount of charge carriers was promoted. From these photocurrent densities it is possible to calculate the overall solar to hydrogen efficiency (STH), without the need for measuring the production of gas, from the following equation [34, 35]:

$$\eta = \frac{I\,(1.23 - E)}{P_{irradiation}} \qquad (6)$$

Where I is the photocurrent density measured at the applied bias E (versus RHE) and $P_{irradiation}$ is the incident light intensity (100 mW/cm^2). The values of STH efficiency respect to applied potential for each of ZnO films are shown in Figure 10. It is clear to observe in this figure that, for all cases, a maximum efficiency is observed. Figure 10 indicate that at potential values greater than 0.35 V, the efficiency η diminishes. The maximum values for the experimental efficiency η calculated at 0.4 V were 0.65% , 0.35% and 0.33% for ZnO obtained at -1.0, -1.5 and -2.0 mA cm^{-2} at 70 ^{o}C, respectively. In the literature [15, 50, 51] have been reported values of experimental efficiency η for the OER on ZnO nanostructures, which were 0.1 [15], 0.08 [50] and 0.044 % [51]. A comparative analysis, between these results and the reported in this work, indicates that our experimental results of η are

higher than the previously reported. It is important to indicate that the highest experimental efficiency η value, in our case, corresponds to ZnO film with the smallest particle size.

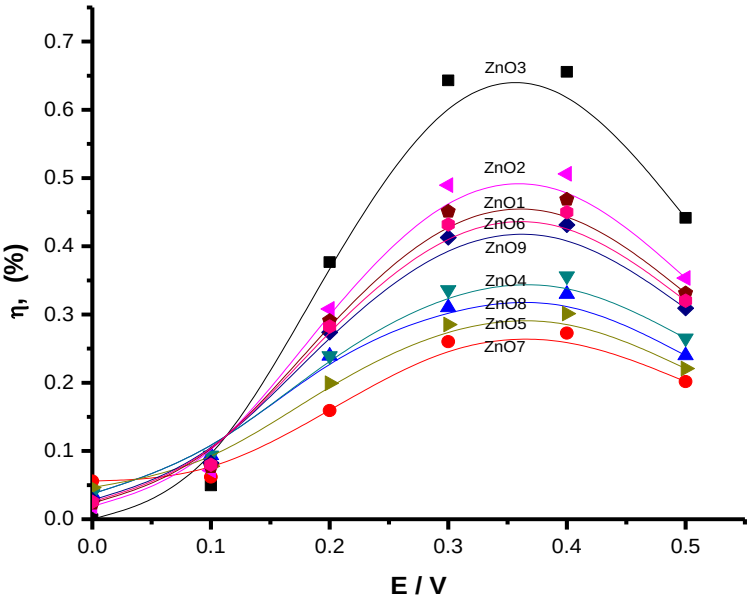

Figure 10. Photoconversion efficiency as function of applied potential at different temperature and applied current: a) ZnO1, b) ZnO2, c) ZnO3, d) ZnO4, e) ZnO5, f) ZnO6, g) ZnO7, h) ZnO8 and i) ZnO9.

4. CONCLUSIONS

In summary, the ZnO films with hexagonal morphology were prepared on ITO substrates by galvanostatic electrodeposition from neutral solution containing acetates. The effect of applied current and solution temperature on the morphological, structural, optical and electrocatalytic properties of the synthesized ZnO films was studied. The SEM images shown that when the current value was smallest and the solution temperature was biggest it is possible to obtain ZnO films with the grain size smallest. The XRD analysis indicated that an increase in the generation of polar planes (002) in ZnO films occur when the synthesis of these is carried out under conditions of the minimum value of cathodic current and of the maximum value of solution temperature. Optical characterization showed that when ZnO films present a small grain size and a big proportion of polar planes to non-polar planes provoke the reduction in the value of band gap due to an increase of the amount of oxygen vacancies. The electrochemical characterization showed that the ZnO films obtained in this work are good electrocatalysts for its application in photoelectrochemical water splitting under solar-simulated irradiation. Calculations of values of overall solar to hydrogen efficiency (STH) associated to photoelectrocatalytic activity for each ZnO film indicated a enhancement in the activity of these for oxygen evolution reaction with respecto to the reported in literature. The high electrocatalytic activity of the ZnO films is associated to two factors: 1) the generation of oxygen vacancies, which allows a

greater caption of light in visible region of solar spectrum; and 2) the decrease in the grain size, which provokes a increase in the electroactive area for OER and a decrease in the recombination rate of hole-electron pair.

ACKNOWLEDGEMENTS
Authors want to thank the financial support for this research to PROMEP through project UPLC-PTC-001. F. D. Ruiz-Ocampo also acknowledge to PROMEP for the scholarship support from project UPLC-PTC-001.

References

1. G. Kreysa, K. Ota, R. F. Savinell, Encyclopedia of Applied Electrochemistry, Springer (2014) New York, USA
2. Southampton Electrochemistry Group, Instrumental Methods in Electrochemistry, Ellis Horwood Ltd. (1985) Chichester, England
3. Damjanovic A, Dey A, Bockris JOM, Electrochim Acta 11 (1966) 791
4. Miles MH, Klaus EA, Gunn BP, Locker JR, Serafin WE, Srinivasan S, *Electrochim. Acta* 23 (1978) 521
5. Bockris JO, Huq AKMS, *Proc. R Soc. London Ser-A* 237 (1956) 277
6. Rossmeisl J, Qu ZW, Zhu H, Kroes GJ, Nørskov JK, *J. Electroanal. Chem* 607 (2007) 83
7. Trasatti S, *Electrochim. Acta* 29 (1984) 1503
8. Tseung ACC, Jasem S, *Electrochim. Acta* 22 (1977) 31
9. Davidson CR, Kissel G, Srinivasan S, *J. Electroanal. Chem*. 132 (1982) 129
10. Singh RN, Hamdani M, Koenig JF, Poillerat G, Gautier JL, Chartier P, *J. Appl. Electrochem*. 20 (1990) 442
11. Jing Jiang, Ailing Zhang, Lili Li, Lunhong Ai, *J. Power Sources* 278 (2015) 445
12. Duck Hyun Youn, Yoon Bin Park, Jae Young Kim, Ganesan Magesh, Youn Jeong Jang, Jae Sung Lee, *J. Power Sources* 294 (2015) 473
13. Dongyu Xu, Yichuan Rui, Yaogang Li, Qinghong Zhang, Hongzhi Wang, *Appl. Surface Sci*. 358 (2015) 436
14. Shannon Klaus, Yun Cai, Mary W. Louie, Lena Trotochaud, and Alexis T. Bell, J. Phys. Chem. C, 119 (2015) 7243
15. R. Lv, T. Wang, F. Su, P. Zhang, C. Li, J. Gong, *Nano Energy* 7 (2014) 143
16. C.-H. Hsu, D.-H. Chen, *Int. J. Hydrogen Energy* 36 (2011) 15538
17. Y. Li, Z. Liu, Y. Wang, Z. Liu, J. Han, J. Ya, *Int. J. Hydrogen Energy* 37 (2012) 15029
18. Z. Bai, X. Yan, Z. Kang, Y. Hu, X. Zhang, Y. Zhang, *Nano Energy* 14 (2014) 392
19. Y.-K. Hsu, S.-Y. Fu, M.-H. Chen, Y.-C. Chen, Y.-G. Lin, *Electrochim. Acta* 120 (2014) 1
20. B. Kumari, S. Sharma, N. Singh, A. Verma, V.R. Satsangi, S. Dass, *Int. J. Hydrogen Energy* 39 (2014) 18216
21. K. H. Ye, J. Y. Wang, N. Li, Z. Q. Liu, S. H. Guo, Y. P. Guo, *Inorg. Chem. Commun*. 45 (2014) 116
22. A. Kushwaha, M. Aslam, *Electrochim. Acta*. 130 (2014) 222
23. M. Skompska, K. Zarębska, *Electrochim. Acta*. 127 (2014) 467
24. J. Wang, Z. Wang, B. Huang, Y. Ma, Y. Liu, X. Qin, *ACS Appl. Mater. Interfaces* 4 (2012) 4024
25. Y. Lv, C. Pan, X. Ma, R. Zong, X. Bai, Y. Zhu, *Appl. Catal. B Environ*. 138-139 (2013) 26
26. Z.L. Wang, *J. Phys. Condens. Matter*. 16 (2004) R829
27. Z.L. Wang, *Mater. Today* 7 (2004) 26
28. C. Jagadish, S.J. Pearton, Zinc Oxide Bulk, Thin Films and Nanostructures: Processing, Properties and Applicationes, Elsevier (2006) Amsterdam, Netherlands

29. X. Xu, D. Chen, Z. Yi, M. Jiang, L. Wang, Z. Zhou, X. Fan, Y. Wang, D. Hui, *Langmuir* 29 (2013) 5573
30. A.I. Inamdar, S.H. Mujawar, S.B. Sadale, A.C. Sonavane, M.B. Shelar, P.S. Shinde, *Sol. Energy Mater. Sol. Cells* 91 (2007) 864
31. A.I. Inamdar, S.H. Mujawar, S.R. Barman, P.N. Bhosale, P.S. Patil, *Semicond. Sci. Technol.* 23 (2008) 085013
32. A.I. Inamdar, S.H. Mujawar, V. Ganesan, P.S. Patil, *Nanotechnology*, 19 (2008) 325706
33. Q. Hou, L. Zhu, H. Chen, H. Liu, W. Li, *Electrochim. Acta* 94 (2013) 72
34. Z. Chen, H.N. Dinh, E. Miller, Photoelectrochemical Water Splitting: Standards, Experimental Methods, and Protocols, Springer-Verlag (2013) New York, USA
35. R. van de Krol, M. Grätzel, Photoelectrochemical Hydrogen Production, Springer USA (2012), New York, USA
36. R. Chang, Chemistry, McGraw-Hill (1999), San Francisco, CA, USA
37. M. Smith, A.E. Martell, Critical Stability Constants, Plenum (1989) New York, USA
38. D.D. Perrin, Stability Constants of Metal-ion Complexes, Pergamon (1979) Oxford, England
39. J.C. Ballesteros, E. Chaînet, P. Ozil, G. Trejo, Y. Meas, *Electrochim. Acta* 56 (2011) 5443
40. S. Peulon, D. Lincot, *J. Electrochem. Soc.* 145 (1998) 864
41. R. Salazar, C. Lévy-Clément, V. Ivanova, *Electrochim. Acta*. 78 (2012) 547
42. F.B. Nişancı, T. Öznülüer, Ü. Demir, *Electrochim. Acta* 108 (2013) 281
43. S. Taguchi, M. Kondo, H. Mori, A. Aramata, *Electrochim. Acta* 111 (2013) 642
44. R. Schlaf , H. Murata , Z.H. Kafafi, J. of Electron Spectroscopy and Related Phenomena 120 (2001) 149
45. D. Kolb, in: H. Gerischer, C.W. Tobias, Advances in Electrochemistry and Electrochemical Engineering, Wiley-Interscience (1978) New York, USA
46. G. Li, T. Hu, G. Pan, T. Yan, *J. Phys. Chem*. C. 112 (2008) 11859
47. A.B. Patil, K.R. Patil, S.K. Pardeshi, *J. Solid State Chem*. 184 (2011) 3273
48. X. Q. Meng, D. Z. Shen, J. Y. Zhang, D. X. Zhao, Y. M. Lu, *Solid State Commun*. 135 (2005) 179
49. J. Zhou, Y. Wang, F. Zhao, Y. Wang, Y. Zhang, L. Yang, *J. Lumin*. 119-120 (2006) 248
50. M. Liu, C. Y. Nam, C. T. Black, J. Kamcev and L. Zhang, *J. Phys. Chem*. C 117 (2013) 13396
51. S. Hernández, V. Cauda, D. Hidalgo, V. Farías-Rivera, D. Manfredi, A. Chiodoni, F. C. Pirri, *J. Alloys Comp*. 615 (2014) S530